J. Fluid Mech. (2003), *vol.* 496, *pp.* 105–127.
DOI: 10.1017/S0022112003006359 Printed in the United Kingdom

Effect of surfactants on film flow down a periodic wall

By C. POZRIKIDIS

Department of Mechanical and Aerospace Engineering, University of California, San Diego, La Jolla, CA 92093-0411, USA
cpozrikidis@ucsd.edu

(Received 23 October 2002 and in revised form 20 June 2003)

The effect of an insoluble surfactant on the gravity-driven flow of a liquid film down an inclined wall with periodic undulations or indentations is investigated in the limit of vanishing Reynolds number. A perturbation analysis for walls with small-amplitude sinusoidal corrugations reveals that the surfactant amplifies the deformation of the film surface, though it also renders the film thickness more uniform over the inclined surface. The effect of the surfactant is most significant when the film thickness is less than half the wall period. To explain the deforming influence of the surfactant, a linear stability analysis of film flow down an inclined plane is undertaken for two-dimensional perturbations. The results reveal the occurrence of a Marangoni normal mode whose rate of decay is lower than that of the single mode occurring in the absence of surfactants. Numerical methods based on a combined boundary-element/finite-volume method are implemented to compute flow down a periodic wall with large-amplitude corrugations or semi-circular depressions. In the case of a wavy wall, it is found that the shape of the film surface is described well by the linear perturbation expansion for small and moderate wave amplitudes. Streamline patterns reveal that, although the effect of the surfactant on the shape of the film surface is generally small, Marangoni tractions may have a profound influence on the kinematics by causing the onset of regions of recirculating flow.

1. Introduction

The gravity-driven flow of a liquid film down an uneven surface and the centrifugal-driven flow of a liquid layer over a spinning substrate are of interest in a broad range of engineering applications. In industrial practice, corrugated surfaces are used to enhance the rate of heat and mass transport by inducing forced convection and simultaneously generating a large surface area across which transport can take place. Thin-film flows are encountered in the manufacturing of microelectronics components, cathode ray tubes, active glass screens, computer disks and magnetic tapes, and are the centrepiece of industrial and household painting and photographic emulsion coating technology.

Laboratory and theoretical studies have shown that film flows are sensitive to the substrate geometry, Reynolds number, and capillary number expressing the effect of surface tension. Asymptotic and numerical solutions of the free-boundary problem describing steady two-dimensional film flow down a wavy wall have been computed by a variety of methods by Wang (1981, 1984), Pozrikidis (1988), Bontozoglou, Kalliadasis & Karabelas (1991), Kang & Chen (1995), Trifonov (1998) and

Malamataris & Bontozoglou (1999). Flow conditions investigated in these studies range from creeping to potential flow, the latter approximating boundary-layer flow with a flat outer velocity profile. Studies of film flow over a wall with two-dimensional topography were conducted by Sukanek (1989), Stillwagon & Larson (1990), Peurrung & Graves (1991), Schiltz (1995), and Kalliadasis, Bielarz & Homsy (2000) based on the lubrication approximation, and by Pozrikidis (1988) and Mazouchi & Homsy (2001) based on the unsimplified equations of Stokes flow. Laboratory investigations have been presented by Zhao & Cerro (1992), Shetty & Cerro (1993, 1998), and more recently by Vlachogiannis & Bontozoglou (2002).

Other studies have investigated film flow down a plane wall over a localized irregularity, with the main goal of providing estimates for the intensity and spatial decay of perturbations. Hansen (1986, 1991) computed free-surface profiles of two-dimensional flow over a cylindrical singly-or doubly-humped protuberance and illustrated the significance of the wall topography and the effect of surface tension. Pritchard, Scott & Tavener (1992) and Abergel & Bona (1992) performed an asymptotic analysis of the decay of localized perturbations, presented numerical solutions of the lubrication equations describing thin-film flow, and compared the theoretical predictions with laboratory observations. Pozrikidis & Thoroddsen (1991) and more recently Lammers, O'Brien & Decrè (1997), Hayes, O'Brien & Lammers (2000) and Decré & Baret (2003) investigated three-dimensional film flow over a cavity or small particle attached to an inclined plane and described the film thickness non-uniformity.

Surfactants are known to play an important role in the structure and dynamics of film flows in a variety of contexts. Their significance of the stability of film flow down an inclined plane has been recognized and investigated by several authors, as reviewed by Ji & Setterwall (1994). In previous studies of film flow down a corrugated or imperfect wall, the effect of surfactants was overlooked and the surface tension was assumed to be uniform over the film surface. The present study will demonstrate that the presence of an insoluble surfactant may have a destabilizing influence in the sense of promoting the film deformation in the limit of creeping flow. This curious finding will be corroborated by a stability analysis of flow down a plane wall in the presence of surfactants, revealing the existence of a Marangoni normal mode whose rate of decay is lower than that of the normal mode arising in the absence of surfactants. The theoretical predictions will be further confirmed by numerical computations using the boundary-element method for finite-amplitude motions and arbitrary wall geometries.

Frenkel & Halpern (2002) and Halpern & Frenkel (2003) discovered that the presence of an insoluble surfactant in two-layer channel flow may induce a Marangoni instability even under conditions of Stokes flow. Conversely, a stationary interface populated with an insoluble surfactant may develop growing waves as soon as a shear flow is imposed. Blyth & Pozrikidis (2003) confirmed the occurrence of the unstable Marangoni normal mode and described the nonlinear stages of the instability by numerical simulation. These recent findings provide direct evidence for the destabilizing influence of a surfactant in an otherwise stable flow, consistent with the conclusions of the present work.

2. Problem statement and governing equations

Consider the flow of a liquid film down a periodic wall with arbitrary geometry in the presence of an insoluble surfactant, as illustrated in figure 1. We will assume that the Reynolds number of the flow defined with respect to the film thickness or period

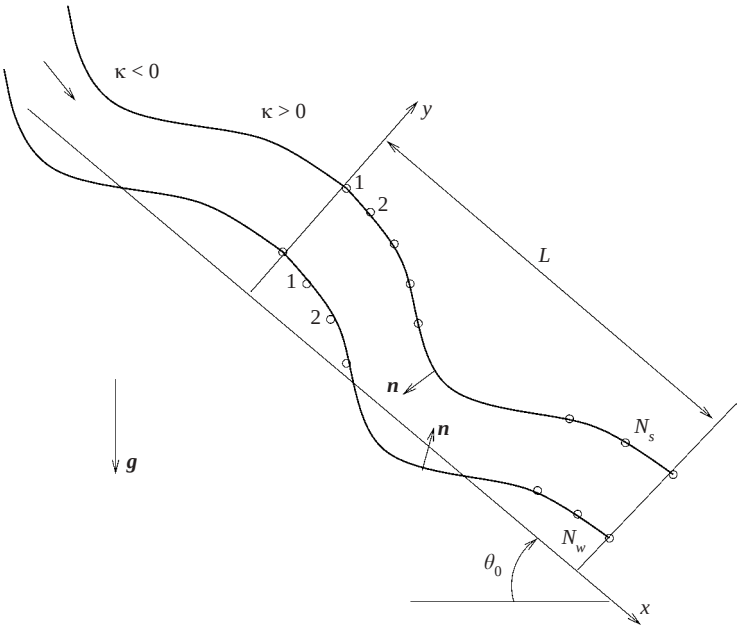

FIGURE 1. Schematic illustration of film flow down an inclined periodic wall with arbitrary geometry.

of the wall is so small that the motion of the fluid is governed by the linear equations of Stokes flow including the Stokes equation and the continuity equation,

$$-\nabla p + \mu\nabla^2 \boldsymbol{u} + \rho \boldsymbol{g} = \boldsymbol{0}, \qquad \nabla \cdot \boldsymbol{u} = 0, \tag{2.1}$$

where μ and ρ are the liquid viscosity and density, $\boldsymbol{u} = (u_x, u_y)$ is the velocity, p is the pressure, and $\boldsymbol{g}$ is the acceleration due to gravity.

The velocity is required to satisfy the no-slip and no-penetration boundary condition, $\boldsymbol{u} = \boldsymbol{0}$ over the wall, and the traction $\boldsymbol{f}$ is required to satisfy the dynamic boundary condition

$$\boldsymbol{f} = \boldsymbol{\sigma} \cdot \boldsymbol{n} = -(\gamma\kappa + p_a)\boldsymbol{n} - \frac{\partial \gamma}{\partial l}\boldsymbol{t}, \tag{2.2}$$

along the film surface, where $\boldsymbol{\sigma}$ is the Newtonian stress tensor, γ is the surface tension, $\boldsymbol{n}$ is the unit normal vector pointing into the film, $\boldsymbol{t}$ is the unit tangential vector pointing in the direction of increasing arclength l, p_a is the ambient pressure, and κ is the surface curvature in the (x, y)-plane reckoned to be positive when the surface is downward parabolic, as illustrated in figure 1.

The surface tension γ is a function of the surfactant concentration Γ. The evolution of the latter is governed by the convection–diffusion equation

$$\frac{\mathrm{d}\Gamma}{\mathrm{d}t} + \frac{\partial (u_t \Gamma)}{\partial l} = -\Gamma\kappa u_n + D_s \frac{\partial^2 \Gamma}{\partial l^2}, \tag{2.3}$$

where $u_t = \boldsymbol{u} \cdot \boldsymbol{t}$ is the tangential velocity, $u_n = -\boldsymbol{u} \cdot \boldsymbol{n}$ is the outward normal velocity, and D_s is the surfactant diffusivity (e.g. Li & Pozrikidis 1997; Pozrikidis 1998, 2001). The derivative $\mathrm{d}/\mathrm{d}t$ on the left-hand side of (2.3) expresses the rate of change of a variable following the motion of interfacial marker points moving with the component of the fluid velocity normal to the film surface. When the marker points also move

tangentially to the film surface, an additional term appears on the right-hand side of (2.3) (e.g. Li & Pozrikidis 1997; Yon & Pozrikidis 1998). In the case of steady flow, the first terms on the left- and right-hand sides of (2.3) vanish, and the two surviving terms express a balance between interfacial convection and diffusion.

When the surfactant concentration is below the saturation level, a linear relationship may be assumed between the surface tension and the surfactant concentration according to Gibbs, $\gamma_c - \gamma = \Gamma RT$, where R is the ideal gas constant, T is the absolute temperature and γ_c is the surface tension of a clean interface that is devoid of surfactants (e.g. Adamson 1990). Rearranging, we obtain the linear equation of state

$$\gamma = \gamma_c \left(1 - \beta \frac{\Gamma}{\Gamma_0} \right), \tag{2.4}$$

where $\beta = \Gamma_0 RT/\gamma_c$ is a dimensionless constant, related to the surface elasticity employed in the surfactant literature by $E = \gamma_c \beta/\Gamma_0$, and Γ_0 is a reference surfactant concentration. More generally, the surface elasticity is defined as $E = -\partial\gamma/\partial\Gamma$. For small variations in the surfactant concentration around the reference value Γ_0, a Taylor series expansion yields $\gamma = \gamma_0 - E(\Gamma - \Gamma_0)$, where $E = -(\partial\gamma/\partial\Gamma)_{\Gamma_0}$.

3. Small-amplitude sinusoidal undulations

Consider steady flow down a wall with small-amplitude sinusoidal corrugations of period L, inclined at the angle θ_0 with respect to the horizontal. In the inclined system of coordinates depicted in figure 1, the wall geometry is described by the real or imaginary part of the function

$$y_w(x) = \epsilon h e^{ikx}, \tag{3.1}$$

where ϵ is a dimensionless coefficient whose magnitude is much less than unity, h is the mean film thickness, i is the imaginary unit, and $k = 2\pi/L$ is the wavenumber. The location of the film surface is described by the corresponding function

$$y_s(x) = h + \epsilon\eta(x) = h(1 + \epsilon A e^{ikx}), \tag{3.2}$$

where A is the dimensionless complex surface amplitude, and $\eta(x) = hAe^{ikx}$ is the wave form of the perturbation. The distribution of the surfactant concentration and surface tension along the film surface are described by the companion functions

$$\begin{aligned} \Gamma(x) &= \Gamma^{(0)} + \epsilon\Gamma^{(1)}(x) = \Gamma_0(1 + \epsilon C e^{ikx}), \\ \gamma(x) &= \gamma^{(0)} + \epsilon\gamma^{(1)}(x) = \gamma_0(1 + \epsilon D e^{ikx}), \end{aligned} \tag{3.3}$$

where $\Gamma^{(0)} = \Gamma_0$ and $\gamma^{(0)} = \gamma_0$ are the uniform values corresponding to the flat-film Nusselt flow, $\Gamma^{(1)} = \Gamma_0 C e^{ikx}$, $\gamma^{(1)} = \gamma_0 D e^{ikx}$, and C, D are dimensionless complex amplitudes. Since the perturbations are assumed small, we can write $D = -Ma\,C$, where

$$Ma = \frac{E\Gamma_0}{\gamma_0} = \frac{\beta}{1 - \beta}, \tag{3.4}$$

is the Marangoni number. The dimensionless coefficient β, applicable for dilute surfactants, was defined in equation (2.4).

To describe the effect of the corrugations, we introduce the streamfunction ψ defined by the equations $u_x = \partial\psi/\partial y$, $u_y = -\partial\psi/\partial x$, and expand the velocity, streamfunction,

and pressure in the perturbation series

$$\left.\begin{aligned} &\boldsymbol{u}(x,y)=\boldsymbol{u}^{(0)}(x,y)+\epsilon\boldsymbol{u}^{(1)}(x,y)+\ldots, \quad \psi(x,y)=\psi^{(0)}(x,y)+\epsilon\psi^{(1)}(x,y)+\ldots,\\ &p(x,y)=p^{(0)}(x,y)+\epsilon p^{(1)}(x,y)+\ldots. \end{aligned}\right\} \tag{3.5}$$

The leading-order terms $\boldsymbol{u}^{(0)}$, $\psi^{(0)}$ and $p^{(0)}$ correspond to the flat-film Nusselt solution, and are given by

$$\left.\begin{aligned} &u_x^{(0)}=\frac{\rho g\sin\theta_0}{2\mu}y(2h-y), \quad u_y^{(0)}=0, \quad \psi^{(0)}=\frac{\rho g\sin\theta_0}{2\mu}y^2\left(h-\tfrac{1}{3}y\right),\\ &p^{(0)}=\rho g\cos\theta_0(h-y)+p_a, \end{aligned}\right\} \tag{3.6}$$

where $g=|\boldsymbol{g}|$ is the magnitude of the acceleration due to gravity. Linearizing the governing equations with respect to ϵ, we find that $\psi^{(1)}(x,y)$ is a biharmonic function, $\nabla^4\psi^{(1)}=0$. Setting $\psi^{(1)}=U_s h f(\hat{y})\exp(\mathrm{i}kx)$, where $U_s=u_x^{(0)}(y=h)=\rho g h^2\sin\theta_0/(2\mu)$ is the Nusselt surface velocity and $\hat{y}=y/h$, we find

$$f(\hat{y})=a_1\mathrm{e}^{\hat{k}\hat{y}}+a_2\hat{y}\mathrm{e}^{\hat{k}\hat{y}}+a_3\mathrm{e}^{-\hat{k}\hat{y}}+a_4\hat{y}\mathrm{e}^{-\hat{k}\hat{y}}, \tag{3.7}$$

where $\hat{k}=kh$, and a_i, $i=1,\ldots,4$, are four dimensionless complex coefficients. The no-penetration and no-slip boundary conditions over the wall require, respectively, $f(0)=0$ and $f'(0)=-2$, where a prime denotes a derivative with respect to $\hat{y}$. Kinematic compatibility requires $\mathrm{D}(y-y_s)/\mathrm{D}t=0$, where $\mathrm{D}/\mathrm{D}t$ is the material derivative; upon substitution, we find that the complex amplitude of the film surface is related to the surface value of the perturbation streamfunction by $A=-f(1)$.

The linearized form of the surfactant transport equation (2.3) in the general case of unsteady flow is

$$\frac{\partial\Gamma^{(1)}}{\partial t}+u_x^{(0)}\frac{\partial\Gamma^{(1)}}{\partial x}+\Gamma^{(0)}\left(\frac{\partial u_x^{(1)}}{\partial x}+\frac{\partial u_x^{(0)}}{\partial y}\frac{\mathrm{d}\eta}{\mathrm{d}x}\right)=D_s\frac{\partial^2\Gamma^{(1)}}{\partial x^2}, \tag{3.8}$$

where all terms are evaluated at $y=h$ (Frenkel & Halpern 2002; Halpern & Frenkel 2003). Note that the second term in the parentheses on the left-hand side of (3.8) arises from the derivative $\partial u_x^{(0)}/\partial l\simeq(\partial u_x^{(0)}/\partial y)(\mathrm{d}y_s/\mathrm{d}x)=\epsilon(\partial u_x^{(0)}/\partial y)(\mathrm{d}\eta/\mathrm{d}x)$. Because, however, the shear stress and thus slope of the Nusselt velocity profile vanishes at the film surface, this term does not make a contribution. On the contrary, in the case of two-layer channel flow considered by Frenkel & Halpern (2002), Halpern & Frenkel (2003) and Blyth & Pozrikidis (2003), the unperturbed interfacial shear stress is generally non-zero. Substituting the preceding expressions into the steady-state version of (3.8), we find that the complex amplitude of the surfactant concentration is given by $C=-f'(1)/(1-2\pi\mathrm{i}/Pe)$, where

$$Pe=\frac{LU_s}{D_s} \tag{3.9}$$

is the surfactant surface Péclet number. Correspondingly, the complex amplitude of the surface tension is given by $D=Ma\,f'(1)/(1-2\pi\mathrm{i}/Pe)$, where Ma is the Marangoni number.

The tangential and normal components of the dynamic boundary condition (2.2) at the film surface may be linearized in a standard way (e.g. Pozrikidis 1997, pp. 466–472). The linearized normal component of the interfacial stress balance

reads

$$\left(p^{(1)}\right)_{y=h} = 2\mu\left(\frac{\partial u_y^{(1)}}{\partial y}\right)_{y=h} + \rho g\cos\theta_0\eta(x) - \gamma^{(0)}\frac{\partial^2\eta}{\partial x^2} + \gamma^{(1)}\kappa^{(0)}. \tag{3.10}$$

Note that, because the interface is flat in the unperturbed configuration, $\kappa^{(0)} = 0$, the last term on the right-hand side vanishes. Consequently, surface tension variations do not affect the normal force balance. Differentiating (3.10) with respect to x and using the tangential projection of the equation of motion to evaluate the pressure derivative on the left-hand side, we obtain the preferred pressure-free form

$$\left(\frac{\partial p^{(1)}}{\partial x}\right)_{y=h} = \mu\nabla^2 u_x^{(1)} = 2\mu\left(\frac{\partial^2 u_y^{(1)}}{\partial x\partial y}\right)_{y=h} + \rho g\cos\theta_0\frac{\partial\eta}{\partial x} - \gamma^{(0)}\frac{\partial^3\eta}{\partial x^3}. \tag{3.11}$$

The complementary linearized tangential component of the interfacial force balance reads

$$\mu\left(\frac{\partial u_x^{(1)}}{\partial y} + \frac{\partial u_y^{(1)}}{\partial x}\right)_{y=h} = 2\frac{\mu U_s}{h^2}\eta + \frac{\partial\gamma^{(1)}}{\partial x}. \tag{3.12}$$

The last term on the right-hand side represents the effect of the Marangoni traction.

Compiling the two scalar wall conditions, the two scalar surface conditions and equation $D = Maf'(1)/(1 - 2\pi\mathrm{i}/Pe)$ derived after (3.9), we find $a_3 = -a_1$, and derive the linear algebraic system $\boldsymbol{M}\cdot\boldsymbol{z} = \boldsymbol{q}$, where $\boldsymbol{z} = [a_1, a_2, a_4, D]^T$ and $\boldsymbol{q} = [-2, 0, 0, 0]^T$. The coefficient matrix $\boldsymbol{M}$ is given by

$$\boldsymbol{M} = \begin{bmatrix} 2\hat{k} & 1 & 1 & 0 \\ (1-q)(\hat{k}^2+1) & \hat{k}^2+\hat{k}+1 & q(\hat{k}^2-\hat{k}+1) & -\dfrac{2\pi^2\mathrm{i}}{Ca\,\hat{k}}\mathrm{e}^{-\hat{k}} \\ \hat{k}^2(1+q)-\mathrm{i}\tau(1-q) & \hat{k}^2-\mathrm{i}\tau & -q(\hat{k}^2+\mathrm{i}\tau) & 0 \\ Ma\,\hat{k}(1+q) & Ma(1+\hat{k}) & Ma\,q(1-\hat{k}) & -\left(1-\dfrac{2\pi\mathrm{i}}{Pe}\right)\mathrm{e}^{-\hat{k}} \end{bmatrix}, \tag{3.13}$$

where $q \equiv \exp(-2\hat{k})$,

$$\tau \equiv \cot\theta_0 + \frac{2\pi^2}{Ca}, \tag{3.14}$$

and

$$Ca \equiv \frac{\mu U_s}{\gamma_0}\left(\frac{L}{h}\right)^2 = \frac{\rho g\sin\theta_0 L^2}{2\gamma_0} \tag{3.15}$$

is the capillary number expressing the magnitude of viscous stresses, $\mu U_s/h$, relative to the capillary pressure, $h\gamma_0/L^2$. Note that, in estimating the capillary pressure, the surface curvature has been scaled with h/L^2.

Five dimensionless parameters are involved in the matrix $\boldsymbol{M}$, including $\hat{k}$, θ_0, Ca, Ma and Pe. When the Marangoni number vanishes, the coefficient D becomes indeterminate, and only the first three equations involving the dimensionless group τ, but not Ca alone, are relevant to the dynamics. Following accepted practice, we introduce the property group

$$\alpha = \frac{\gamma_0 L}{\mu D_s}, \tag{3.16}$$

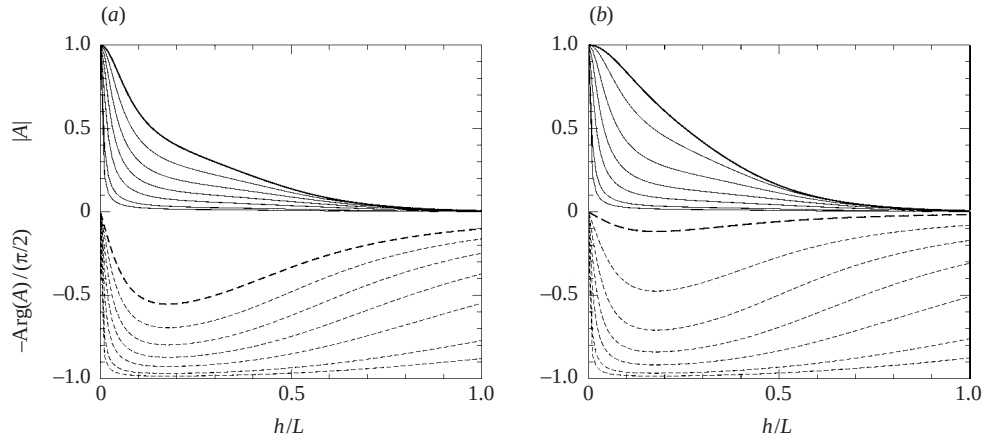

FIGURE 2. Predictions of linear theory for a sinusoidal wall in the absence of surfactants: effect of film thickness on the magnitude (solid lines) and phase shift of the surface wave with respect to the wall (dashed lines), for $Ca = \infty$ (heavy lines), 5, 2, 1, 0.5, 0.2 and 0.1. The inclination angle is (*a*) $\theta_0 = \pi/20$, (*b*) $\pi/4$; in both cases, the phase shift has been reduced by $\pi/2$.

expressing the significance of the surfactant diffusivity, and relate the capillary number to the Péclet number and vice versa by

$$Ca = \frac{Pe}{\alpha}\left(\frac{L}{h}\right)^2, \qquad Pe = \alpha Ca\left(\frac{h}{L}\right)^2. \tag{3.17}$$

The flow may then be studied as a function of h/L, θ_0, Ca expressing the significance of the surface tension, β or Ma expressing the sensitivity of the surface tension on the surfactant concentration, and α.

The perturbation expansion of Wang (1981) demonstrated the effect of h/L and Ca on the deformation of the free surface in the absence of surfactants, that is, for $\beta = 0$ or $Ma = 0$. His analysis was conducted working in an alternative system of coordinates, and results were presented with respect to a different set of dimensionless parameters. By way of establishing a point of reference for demonstrating the effect of surfactants, in figure 2 we illustrate the dependence of the magnitude and phase shift of the surface wave on film thickness for wall inclination angles $\theta_0 = \pi/20$ and $\pi/4$. In these graphs, the phase shift expressed by $-\mathrm{Arg}(A)$ has been reduced by $\pi/2$. The results show that, as the film thickness tends to zero, the film surface tends to conform with the wall, and thus the film thickness tends to become more uniform. On the other hand, as the film becomes thicker, the amplitude of the free surface decreases and effectively vanishes when $h/L = 1$. Surface tension has a strong influence on both the amplitude and phase shift of the surface deformation. As the wall tends to become horizontal, the magnitude $|A|$ drops to zero increasingly closer to the origin of the h/L axis, and the phase shift drops to $-\pi/2$ in the way of the Heaviside step function.

When the capillary number is large, surface tension plays only a minor role and the surfactant is irrelevant insofar as determining the shape of the film surface. Figure 3 illustrates the effect of a surfactant with low diffusivity, $\alpha = 100$, under conditions where viscous and capillary stresses are comparable, $Ca = 2$, over a broad range of values of the surfactant sensitivity parameter β. The results on the surface wave presented in figure 3(*a*) reveal that the surfactant acts to increase the amplitude of the surface deformation represented by the solid lines, and the effect is most pronounced at low and moderate film thicknesses, $h/L < 0.3$. Moreover, the surfactant acts to

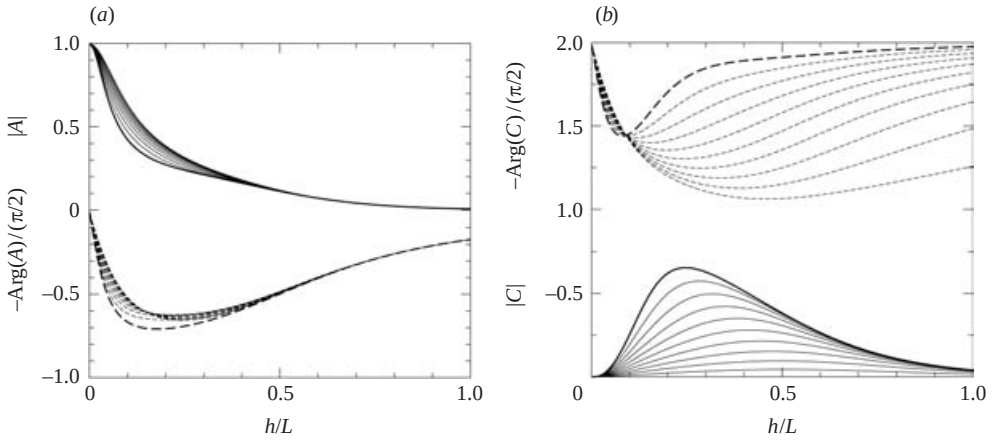

FIGURE 3. Predictions of linear theory for a sinusoidal wall in the presence of surfactants: effect of film thickness on the magnitude (solid lines) and phase shift with respect to the wall (dashed lines), of (*a*) the film surface wave, and (*b*) surfactant concentration wave, for $\theta_0 = \pi/4$, $Ca = 2$, $\alpha = 100$ and $\beta = 0$ (heavy lines), 0.1, 0.2, ..., 0.90. In both graphs, the phase shift has been reduced by $\pi/2$.

decrease the phase shift of the surface deformation with respect to the wall represented by the dashed lines, and thereby renders the film thickness more uniform over the corrugations.

The solid lines in figure 3(*b*) illustrate the behaviour of the surfactant concentration wave, showing that the amplitude of the perturbation represented by the solid lines reaches a maximum at a certain value of h/L that strongly depends on the sensitivity parameter β. That the amplitude of the surfactant concentration tends to zero as the film becomes thicker, $h/L \to \infty$, is expected on the observation that the disturbance flow decays at an exponential rate far from the wall, as can be deduced by inspection of the periodic Green's function of two-dimensional Stokes flow (Pozrikidis 1988). In the opposite limit where the film thickness tends to vanish, the tangential velocity and thus the surfactant concentration tend to become uniform along the film surface.

The dashed lines in figure 3(*b*) show that the phase shift of the surfactant concentration lies in the range $(\pi/2, \pi)$ and reaches a peak at some point between the maximum downward wall slope and immediate trough. If the sinusoidal wall is described by the shape function $y_w(x) = \epsilon h \cos(2\pi x/L)$, then the peak occurs in the interval $L/4 < x < L/2$. This behaviour can be deduced by referring to equation (2.3), and observing that at steady and in the limit of low surfactant diffusivity, only the second term on the left-hand side survives. Integrating with respect to arclength shows that the perturbation in the surfactant concentration is inversely proportional to the tangential surface velocity, which is higher along the downward slope of the wall.

Behaviour similar to that illustrated in figure 3 is observed for different inclination angles. In all cases, the surfactant promotes the surface deformation but also tends to render the film thickness more uniform over the corrugations by reducing the phase shift. When the property group α is lowered to values of the order of unity, surface diffusion dominates and the effect of the surfactants becomes insignificant. For example, when $\theta_0 = \pi/4$, $h/L = 0.10$ and $Ca = 2$, the amplitude of the film surface is $|A| = 0.423$ in the absence of surfactants, $|A| = 0.430$ for $\alpha = 1$ and $\beta = 0.5$, and $|A| = 0.582$ for $\alpha = 100$ and $\beta = 0.5$.

4. Stability of flow down an inclined plane and over a horizontal wall

The linear analysis of § 3 has revealed that surfactants promote the deformation of the film surface in steady flow. However, this does not necessarily imply that surfactants also have a destabilizing influence on the evolution of surface waves in unsteady flow. In fact, previous analysis and laboratory observations for film flow down an inclined plane have provided evidence to the contrary, by demonstrating that adding surfactants raises the critical Reynolds number (film thickness) above which surface waves begin to grow.

To resolve the issue of stability, we consider the evolution of infinitesimal perturbations in the context of Stokes flow. The mathematical formulation of the linear stability problem for flow down a wavy wall involves lengthy derivations that are beyond the scope of the present work (Wei & Rumschitzki 2002). For simplicity then, we confine our attention to flow down an inclined plane wall or over a horizontal wall, but note that the restriction on the planar geometry is not as restrictive as it might appear. Tougou (1978) found that small-amplitude wall corrugations do not affect the stability of long waves.

4.1. *Flow down an inclined wall*

To carry out the normal-mode stability analysis for two-dimensional perturbations, we describe the position of the film surface by the function $y_s(x,t) = h + \epsilon\eta(x,t)$, where ϵ is a small dimensionless coefficient, $\eta(x,t) = hA\exp[\mathrm{i}(kx - \sigma t)])$, A is an arbitrary dimensionless coefficient, and σ is the complex growth rate of a normal mode. The perturbation streamfunction, surfactant concentration, and surface tension are expressed in the corresponding forms

$$\begin{bmatrix} \psi^{(1)} \\ \Gamma^{(1)} \\ \gamma^{(1)} \end{bmatrix} = \begin{bmatrix} U_s h f(\hat{y}) \\ \Gamma_0 C \\ \gamma_0 D \end{bmatrix} \times \exp[\mathrm{i}(kx - \sigma t)], \tag{4.1}$$

where $\hat{y} \equiv y/h$, and the function $f(\hat{y})$ is given in (3.7). Kinematic compatibility requires $A = -f(1)/\zeta$, where $\zeta = 1 - \hat{c}$, $\hat{c} \equiv c/U_s$ and $c = \sigma/k$ is the complex phase velocity. Next, we introduce the wall and film surface conditions and find $a_3 = -a_1$. The remaining complex coefficients satisfy the homogeneous linear system $\boldsymbol{N}\cdot\boldsymbol{z} = \boldsymbol{0}$, where $\boldsymbol{z} = [a_1, a_2, a_4, D]^T$, and the coefficient matrix is given by

$$\boldsymbol{N} = \begin{bmatrix} 2\hat{k} & 1 & 1 & 0 \\ (1-q)(\zeta\hat{k}^2+1) & \zeta\hat{k}^2+\zeta\hat{k}+1 & q(\zeta\hat{k}^2-\zeta\hat{k}+1) & -\zeta\dfrac{2\pi^2\mathrm{i}}{Ca\,\hat{k}}\mathrm{e}^{-\hat{k}} \\ \zeta\hat{k}^2(1+q)-\mathrm{i}\tau(1-q) & \zeta\hat{k}^2-\mathrm{i}\tau & -q(\zeta\hat{k}^2+\mathrm{i}\tau) & 0 \\ Ma\,\hat{k}(1+q) & Ma(1+\hat{k}) & Ma\,q(1-\hat{k}) & -\left(\zeta-\dfrac{2\pi\mathrm{i}}{Pe}\right)\mathrm{e}^{-\hat{k}} \end{bmatrix}. \tag{4.2}$$

As in § 3, $\hat{k} \equiv kh$, $q \equiv \exp(-2\hat{k})$, and the dimensionless groups τ, Ca and Pe are defined in (3.14), (3.15) and (3.9). Six dimensionless parameters are involved in the matrix $\boldsymbol{N}$, including $\hat{k}$, ζ, θ_0, Ca, Ma and Pe. Note that the matrix $\boldsymbol{M}$ defined in (3.13) arises from $\boldsymbol{N}$ by substituting $c = 0$ or $\zeta = 1$, corresponding to a stationary film surface. Setting the

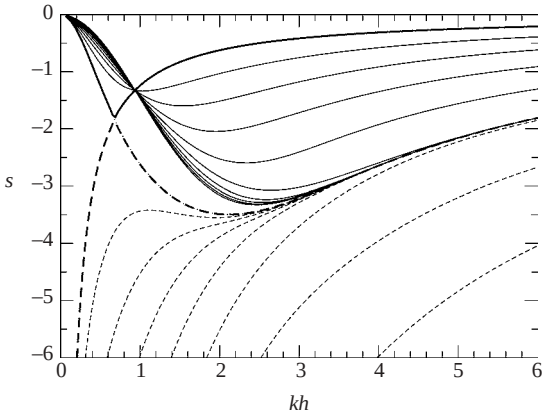

FIGURE 4. Dimensionless growth rate s of surface waves for flow down a plane wall inclined at an angle $\theta_0 = \pi/4$, $Ca = 2$, $\alpha = 100$ and $\beta = 0.001$ (heavy solid and broken lines), 0.1, 0.2, ..., 0.9. The broken lines represent the first normal mode, and the solid lines represent the second normal mode. The hardly visible dotted line represents Yih's mode applicable in the absence of surfactants.

determinant of $\boldsymbol{N}$ equal to zero provides us with a third-order algebraic equation for the computation of the reduced and shifted complex phase velocity ζ. One trivial root is given by $\zeta = 0$ corresponding to $c = U_s$, and the other two roots may be computed in terms of the coefficients of the remainder binomial using the quadratic formula. In practice, the coefficients are extracted by solving a system of complex linear equations for three trial values of ζ. Thus, in the presence of surfactants, the flow admits two normal modes.

In the absence of surfactants, $\beta = 0$ or $Ma = 0$, the coefficient D becomes indeterminate, and only the first three equations in (4.2) involving the dimensionless group τ, but not Ca alone, are relevant to the dynamics. Yih (1963) derived analytical expressions for the phase velocity c_R and rate of decay of surface waves $\sigma_I = kc_I$, where the subscripts R and I denote the real and imaginary part. The dimensionless phase velocity, $v \equiv c_R/U_s$, and dimensionless growth rate, $s \equiv \sigma_I h/U_s = c_I \hat{k}/U_s$, are given by

$$v = 1 + \frac{1}{\cosh^2 \hat{k} + \hat{k}^2}, \qquad s = -\frac{\tau}{2\hat{k}} \frac{\sinh(2\hat{k}) - 2\hat{k}}{\cosh^2 \hat{k} + \hat{k}^2}. \tag{4.3}$$

Since the fraction on the right-hand side of the expression for the growth rate is positive for any $\hat{k}$, the growth rate is negative, and the flow is stable.

Figure 4 displays the dimensionless growth rate s of the two normal modes for $\theta = \pi/4$, $Ca = 2$, $\alpha = 100$ and a range of values of β. The dotted line interwoven with the right-hand portion of the dashed line represents Yih's analytical prediction given in the second equation of (4.3), corresponding to $\beta = 0$. The results reveal that, as soon as β becomes non-zero, Yih's function splits into two parts at the critical point $\hat{k}_c \simeq 0.672$. Two branches corresponding to the two normal modes then arise from the simultaneous splitting of the function $s = \varphi(\hat{k}) = -2\pi\hat{k}/Pe = -8\pi^3/(\alpha Ca\hat{k})$ corresponding to the last element of the matrix $\boldsymbol{N}$. Because the growth rate of the first normal mode described by the dashed lines is lower than that of the Yih mode for any wavenumber, the surfactant has a stabilizing influence. In contrast, because the growth rate of the second mode described by the solid lines is higher than that of the

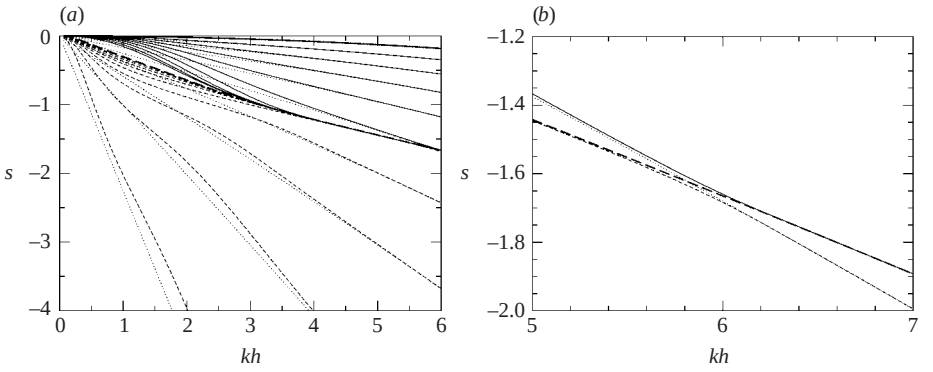

FIGURE 5. (*a*) Dimensionless growth rate s of surface waves for $\theta_0 = \pi/4$, $Ca' = 2$, $\alpha' = 100$ and $\beta = 0.001$ (heavy solid and broken lines), 0.1, 0.2, ..., 0.9. The dotted lines represent the asymptotic form of the Marangoni mode. (*b*) Magnified view for $\alpha = 0.5$ showing the switching of branches of the two normal modes.

Yih mode for any wavenumber, the surfactant has a competing or complementary destabilizing influence. However, it should be emphasized that the growth rates along this branch are negative and the flow is stable.

A further feature of figure 4 is that the graphs of the second mode pass through a pivot point that is located on the graph of the function $s = \varphi(\hat{k})$ at the position $\hat{k}_p = 0.9362$, correct to shown accuracy, with no apparent significance on the behaviour of the first normal mode. Numerical investigation showed that the precise position of the pivot point depends on θ_0, Ca and α. Accordingly, locally near $\hat{k}_p$, the linearized equation determining the growth rate of the second normal mode takes the form $s = f_0(\theta_0, Ca, \alpha) + (\hat{k} - \hat{k}_p) f_1(\theta_0, Ca, \alpha, \beta) + \ldots$, where $f_0 = \varphi(\hat{k}_p)$. Note the absence of β from the arguments of f_0. Mathematically, the imaginary part of the last element of the matrix $\boldsymbol{N}$ vanishes at the pivot point, screening out the Marangoni number that appears only in the last row. Physically, if the wavelength L is kept constant while the film thickness h is increased from values below $\hat{k}_p$ or decreased from values above $\hat{k}_p$, there will be a critical thickness corresponding to $\hat{k}_p$ where the effect of the surfactant will be independent of β or Ma.

Now, because the present analysis was motivated by the problem of film flow down a wavy wall discussed in § 3, the capillary number Ca and property group α have been defined using as characteristic length the wavelength L. In considering flow down a plane wall from the viewpoint of hydrodynamic stability, it is appropriate to redefine these dimensionless groups in terms of the mean film thickness, as

$$Ca' = \frac{\mu U_s}{\gamma_0} = Ca\left(\frac{h}{L}\right)^2, \qquad \alpha' = \frac{\gamma_0 h}{\mu D_s} = \alpha\left(\frac{h}{L}\right). \tag{4.4}$$

Moreover, the growth rate can be reduced with respect to the capillary time scale, $\gamma_0/\mu h$ to give the alternative dimensionless growth rate $s' \equiv \sigma_I \mu h/\gamma_0 = c_I \mu \hat{k}/\gamma_0$, which is related to s by $s' = sCa'$. Figure 5(*a*) shows graphs of the dimensionless growth rate s for $\theta_0 = \pi/4$, $Ca' = 2$, $\alpha' = 100$ and a range of values of β. The dashed lines correspond to the first normal mode and the solid lines correspond to the second normal mode.

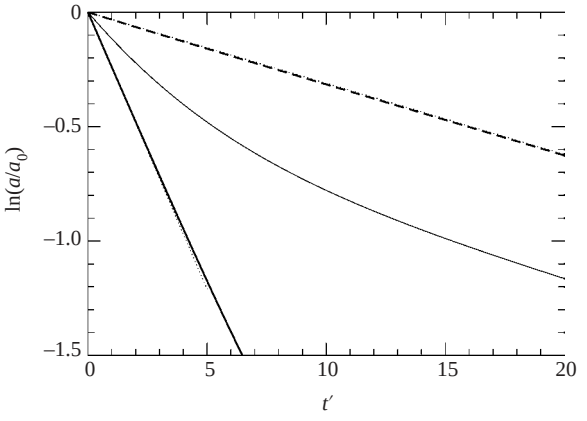

FIGURE 6. Decay of surface waves in film flow down a plane wall inclined at an angle $\theta_0 = \pi/4$, for $h/L = 0.10$, $Ca = 2$, $\beta = 0.25$ and $\alpha = 100$. The heavy solid and dashed lines correspond to the two normal modes, the dotted lines represent the predictions of the linear stability theory, and the intermediate line corresponds to an arbitrary initial condition.

In the limit as $\hat{k}$ tends to infinity while Ca' is held constant, the growth rate of the Yih mode behaves like

$$s \simeq -\frac{\tau}{\hat{k}} \simeq -\frac{\hat{k}}{2\ Ca'} \quad \text{or} \quad s' \simeq -\frac{\hat{k}}{2}, \tag{4.5}$$

whereas the growth rate of the complementary Marangoni mode behaves like

$$s \simeq -\frac{\hat{k}}{Ca'}\left(\frac{\hat{k}}{\alpha'} + \frac{Ma}{2}\right) \quad \text{or} \quad s' \simeq -\hat{k}\left(\frac{\hat{k}}{\alpha'} + \frac{Ma}{2}\right). \tag{4.6}$$

The latter is described by the dotted lines in figure 5. The asymptotic functional forms shown in (4.5) and (4.6) reveal that, to leading order in $\hat{k}$, the growth rate of the Yih mode is independent of the properties of the surfactant, that is, the presence of the surfactant has a negligible effect on the behaviour of the corresponding normal mode. On the other hand, the growth rate of the Marangoni mode is determined by the surfactant diffusivity and is independent of the Marangoni number. The quadratic dependence of the Marangoni growth rate on $\hat{k}$ shown in (4.6) suggests that, unless $D_s = 0$ and $Ma < 1$, this mode will decay faster than the Yih mode at sufficiently high wavenumbers. Accordingly, the dashed lines in figure 5(a) must switch from the Yih branch corresponding to (4.5) over to the Marangoni branch corresponding to (4.6) at a certain value of β; the converse is expected for the solid lines. This transition is confirmed in the amplified scale of figure 5(b) corresponding to $\beta = 0.5$. The heavy broken line represents the growth rate of the Yih mode in the absence of surfactants, and the dotted line represents the asymptotic prediction (4.6).

To confirm independently the existence of two normal modes with the aforementioned properties, we used the boundary-element method discussed in the Appendix to compute the evolution of a small-amplitude wave on the film surface. Results of numerical simulations are displayed in figure 6 for the conditions described in the caption. In this graph, the surface amplitude, a, reduced by the initial value, a_0, is plotted against the reduced time $t' = t\rho gL/\mu$ on a linear-log scale. The slopes of the leftmost heavy solid curve and rightmost heavy dashed curve, corresponding to the two normal modes, are in excellent agreement to the predictions of linear stability

theory represented by the dotted lines, given by -0.24214 and -0.03108. At long times, the intermediate solid curve, corresponding to an arbitrary (non-normal mode) initial condition, tends to become a straight line with a slope that is equal to that of the slower decaying normal mode.

The results of the linear stability analysis presented in this section are consistent with our earlier findings in § 3 concerning the effect of surfactants in steady flow down a wavy wall, as well as with the recent findings of Frenkel & Halpern (2002), Halpern & Frenkel (2003), and Blyth & Pozrikidis (2003) concerning the surfactant-induced instability of two-layer channel flow, as will be discussed in § 6.

4.2. *Film on a horizontal wall*

As the inclination angle tends to zero, the surface velocity vanishes, the scaling underlying (4.1) fails, and the definitions of Ca, τ and ζ are no longer appropriate. To study this limit, we replace (4.1) by

$$\begin{bmatrix} \psi^{(1)} \\ \Gamma^{(1)} \\ \gamma^{(1)} \end{bmatrix} = \begin{bmatrix} \dfrac{\gamma_0 h}{\mu}\phi(\hat{y}) \\ \Gamma_0 C \\ \gamma_0 D \end{bmatrix} \times \exp[\mathrm{i}(kx - \sigma t)], \tag{4.7}$$

and express the function $\phi(\hat{y})$ in the form

$$\phi(\hat{y}) = a_1' \mathrm{e}^{\hat{k}\hat{y}} + a_2' \hat{y} \mathrm{e}^{\hat{k}\hat{y}} + a_3' \mathrm{e}^{-\hat{k}\hat{y}} + a_4' \hat{y} \mathrm{e}^{-\hat{k}\hat{y}}, \tag{4.8}$$

where a_i', $i = 1, \ldots, 4$, are four dimensionless coefficients. Requiring the satisfaction of the wall and film surface conditions, we find $a_3' = -a_1'$. The remaining complex coefficients satisfy the homogeneous linear system $\boldsymbol{N}' \cdot \boldsymbol{z}' = \boldsymbol{0}$, where $\boldsymbol{z}' = [a_1', a_2', a_4', D]^T$, the coefficient matrix is given by

$$\boldsymbol{N}' = \begin{bmatrix} 2\hat{k} & 1 & 1 & 0 \\ (1-q)\hat{k} & \hat{k}+1 & q(\hat{k}-1) & -\mathrm{i}\frac{1}{2}\mathrm{e}^{-\hat{k}} \\ \hat{c}'\hat{k}^2(1+q) + \mathrm{i}\tau'(1-q) & \hat{c}'\hat{k}^2 + \mathrm{i}\tau' & q(-\hat{c}'\hat{k}^2 + \mathrm{i}\tau') & 0 \\ Ma\,\hat{k}(1+q) & Ma(1+\hat{k}) & Ma\,q(1-\hat{k}) & \left(\hat{c}' + \frac{\mathrm{i}\hat{k}}{\alpha'}\right)\mathrm{e}^{-\hat{k}} \end{bmatrix}, \tag{4.9}$$

$\hat{c}' \equiv c\mu/\gamma_0$ is a dimensionless complex phase velocity,

$$\tau' \equiv \frac{\hat{k}^2}{8\pi^2}(Bo + 4\pi^2) = \tfrac{1}{2}(Bo' + \hat{k}^2), \tag{4.10}$$

$Bo \equiv \rho g L^2/\gamma_0$ is the Bond number defined with respect to the wavelength, and $Bo' \equiv \rho g h^2/\gamma_0$ is the Bond number defined with respect to the layer thickness. Setting the determinant of $\boldsymbol{N}'$ to zero provides us with a quadratic equation with two purely imaginary roots for $\hat{c}'$, corresponding to negative growth rates s'. In the limit as $\hat{k}$ tends to infinity, the growth rate of the first mode behaves like $s' \simeq -\hat{k}/2$, and the growth rate of the second mode behaves as $s' \simeq -\hat{k}(\hat{k}/\alpha' + Ma/2)$, in correspondence with (4.5) and (4.6).

In the absence of surfactant, $\beta = 0$ or $Ma = 0$, the coefficient D becomes indeterminate, and only the first three equations in (4.9) involving the dimensionless group τ' are relevant to the dynamics. After some algebra, we find that the real part of the phase velocity is zero, as expected by symmetry, and the dimensionless growth rate is given by the second of (4.3) with s' in place of s and τ' in place of τ. This result is consistent with a more general expression for the growth rate of the Stokes flow

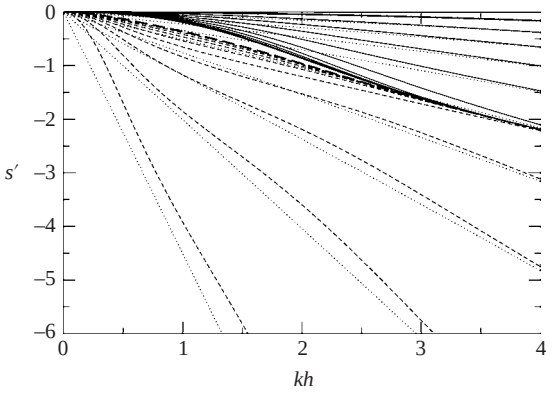

FIGURE 7. Dimensionless growth rate s' of surface waves on horizontal film resting on a plane wall for $Bo' = 2$, $\alpha' = 100$ and $\beta = 0.001$ (heavy solid and broken lines), 0.1, 0.2, ..., 0.9, corresponding to the graphs shown in figure 5(a).

instability of a liquid layer resting on a horizontal wall underneath a semi-infinite fluid of arbitrary viscosity and density, derived by Newhouse & Pozrikidis (1990).

Figure 7 shows graphs of the dimensionless growth rate s' for $Bo' = 2$, $\alpha' = 100$, and $\beta = 0.001$ (heavy solid and broken lines), 0.1, 0.2, ..., 0.9. The general structure of the stability chart is similar to that displayed in figure 5(a), and the expected asymptotic behaviour is borne out from the numerical computation.

5. Boundary-element solutions

To overcome the restrictions on the magnitude of the perturbations imposed by linear theory, a numerical method was implemented for computing unsteady and steady Stokes flow down a periodic wall with arbitrary geometry. In one implementation of the numerical method, the evolution of the film surface was computed using the boundary-integral method outlined in the Appendix, while the convection–diffusion equation for the surfactant concentration was integrated in time using an implicit finite-volume method (Pozrikidis 1998). Simulations were carried out from an arbitrary initial condition, typically involving a flat film surface and a uniform surfactant concentration, until a steady state is established. In another implementation of the numerical method, the equations of steady flow were solved directly using an iterative method. Apart from being less sensitive to the initial condition, the first method for unsteady flow has the added advantage of providing us with information on stability, and was chosen in the majority of the numerical investigations. The simulations showed that, when the initial amplitude of the film surface is sufficiently small, the film tends to a stable steady state at long times under all conditions considered.

5.1. *Sinusoidal walls*

The numerical results for small wall amplitudes are in good agreement with the predictions of the linear perturbation analysis discussed in § 2. For example, when $Ca = 2$, $\beta = 0.6$, $\alpha = 100$ and $h/L = 0.10$, linear analysis predicts $|A| = 0.598$ and $-\mathrm{Arg}(A) = -0.533\pi/2$ for the film surface amplitude, and $|C| = 0.049$ and $-\mathrm{Arg}(C) = 1.417\pi/2$ for the surfactant concentration amplitude. The boundary-integral solution for wall amplitude $\epsilon = a_w/h = 0.10$ with $N_w = 48$ elements over one

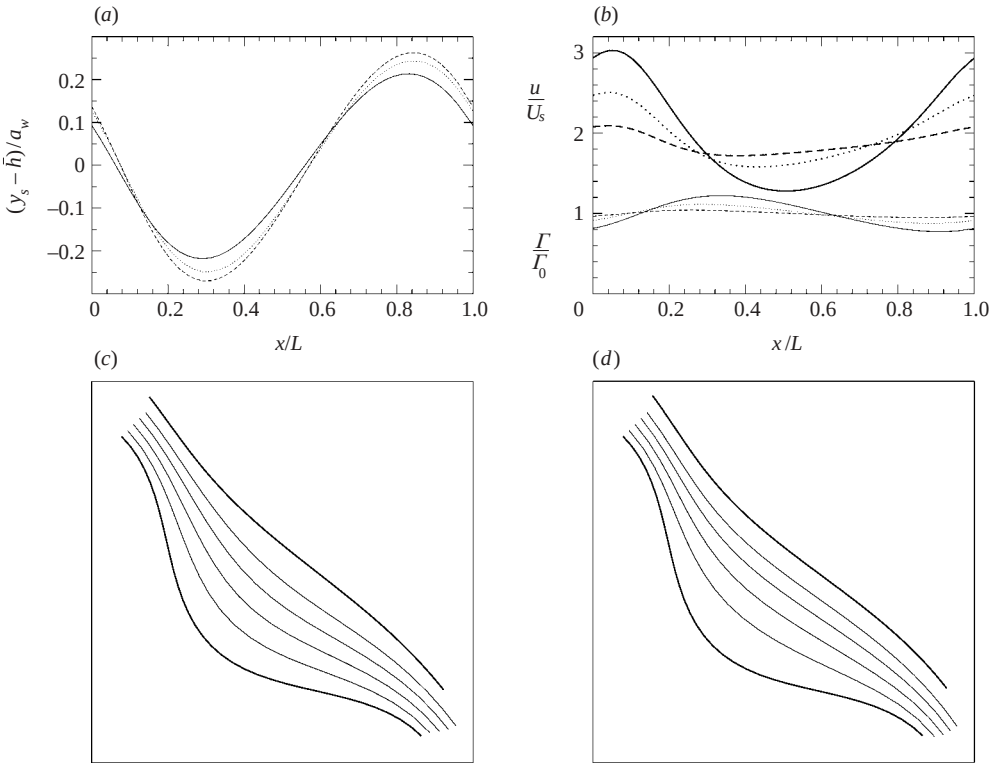

FIGURE 8. (*a*) Effect of surfactant on the film surface for $\theta_0 = \pi/4$, $Ca = 2$, $\alpha = 100$, mean film thickness $\overline{h}/L = 0.20$, wall amplitude $a_w/L = 0.10$ and $\beta = 0.0$ (solid line), 0.2 (dotted line) and 0.5 (dashed line) (*b*) Corresponding distribution of the tangential surface velocity and surfactant concentration, represented by the heavy and light lines. (*c, d*) Streamline patterns for $\beta = 0$ and 0.5.

period of the wall and $N_s = 48$ elements over one period of the film surface, yields $|A| = 0.560$, $-\mathrm{Arg}(A) = -0.542\pi/2$, $|C| = 0.051$ and $-\mathrm{Arg}(C) = 1.358\pi/2$. Considering that the wall amplitude is 10% of the film thickness, we find good agreement with the theoretical predictions.

Moreover, the qualitative effect of the surfactant is described well by linear theory even for non-infinitesimal wall amplitudes. Surfactants amplify the deformation of the film surface, and the effect is most pronounced in the range of film thicknesses suggested by the perturbation analysis. As an example, we consider flow down a wavy wall described by the equation $y_w = a_w \cos(kx)$, for $\theta_0 = \pi/4$, $a_w/L = 0.10$, $Ca = 2$, $\alpha = 100$, and mean film thickness $\overline{h}/L = 0.20$, where $\overline{h} \equiv A/L$ and A is the area of the liquid inside each period. Figure 8(*a*) displays the surface profile y_s shifted by $\overline{h}$ and reduced by the wall amplitude a_w, for $\beta = 0.0$, 0.20, and 0.50, and figure 8(*b*) shows the corresponding distribution of the surfactant concentration (thin lines) and surface velocity (heavy lines), the latter normalized by the Nusselt velocity U_s corresponding to a film thickness $\overline{h} - a_w$.

The distribution of the surfactant concentration can be estimated by recalling that the perturbation in the surfactant concentration is roughly inversely proportional to the tangential surface velocity, and this deduction is consistent with the graphs

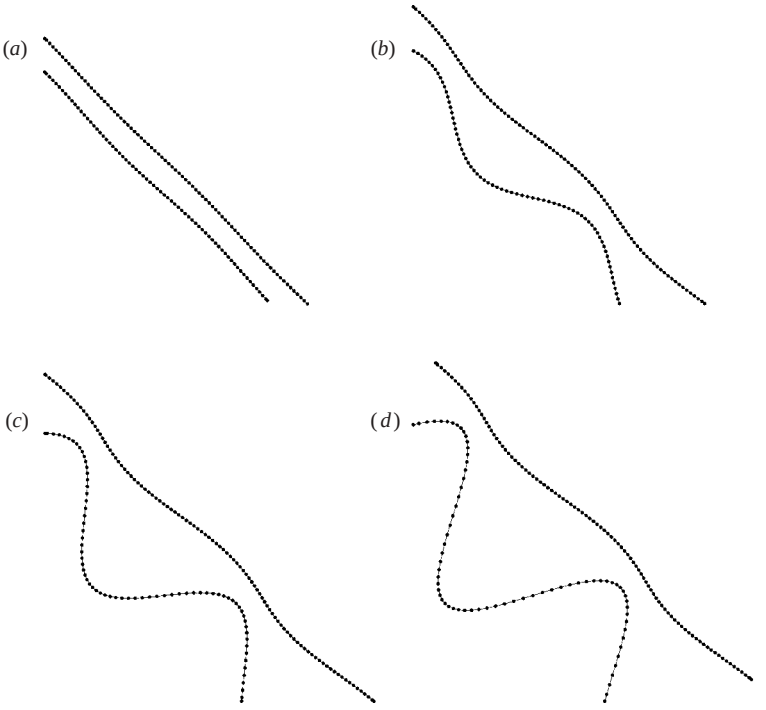

FIGURE 9. Film profiles for $\theta_0 = \pi/4$, $Ca = 2$, $\alpha = 100$, $\beta = 0.5$, reduced mean film thickness $(\bar{h} - a_w)/L = 0.10$, and (*a*) $a_w/L = 0.01$, (*b*) 0.10, (*c*) 0.20 and (*d*) 0.30. The circular symbols mark the location of the wall and surface boundary element nodes.

displayed in figure 8(*b*). Conversely, we recall that the Marangoni traction is proportional to $-\mathrm{d}\Gamma/\mathrm{d}l$, and this suggests that the presence of a surfactant acts to, respectively, slow down or speed up the motion of the fluid over the crests or troughs, and thereby render the tangential velocity uniform over the film surface. Figure 8(*c, d*) shows streamlines originating from evenly spaced points across the film over the crest, for $\beta = 0$ and 0.5, illustrating the significant effect of the surfactant on the structure of the flow. Later in this section, we will see that the surfactant may in fact cause the onset of regions of recirculating flow.

To illustrate the effect of the wall amplitude, in figure 9 we present film profiles for $\theta_0 = \pi/4$, $Ca = 2$, $\alpha = 100$, $\beta = 0.5$, reduced mean film thickness $(\bar{h} - a_w)/L = 0.10$ and several wall amplitudes a_w/L. When a_w/L is roughly greater than 0.05, the depth of the corrugations has a small effect on the shape of the free surface. In contrast, the distribution of the tangential velocity along the film surface, shown in figure 10(*a*), is sensitive to the wall amplitude. In this graph, the tangential velocity has been normalized by the Nusselt surface velocity of a film of thickness h. In particular, as the wall amplitude is increased, the drop in the tangential velocity down the slope of the corrugations is accentuated, and the position of minimum velocity shifts from a point near the trough toward the downward inflection points. Figure 10(*b*), shows the distribution of the surfactant concentration. The hardly visible dotted line represents the prediction of the linear theory for $a_w/L = 0.01$, which is in excellent agreement with the results of the numerical computation. At higher wall amplitudes, linear theory does not adequately capture the stronger effect of the corrugations.

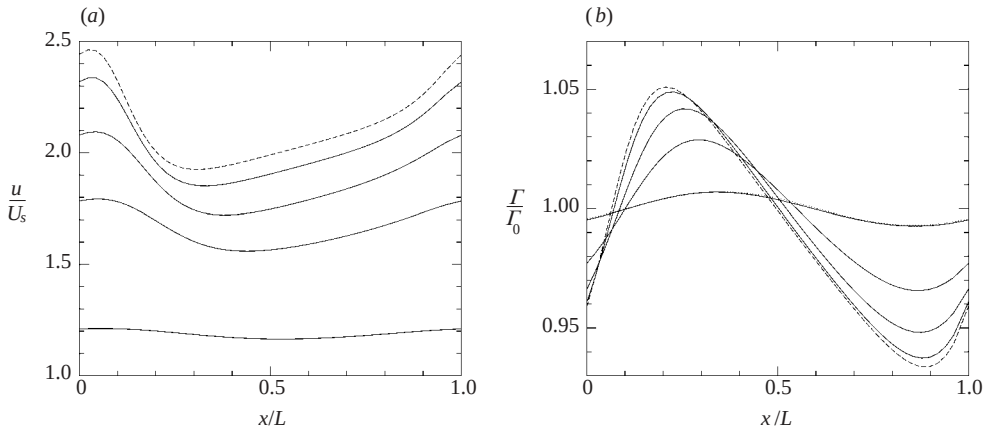

FIGURE 10. Surface distribution of (*a*) the tangential velocity, and (*b*) the surfactant concentration, corresponding to the conditions of figure 9. The wall amplitude is $a_w/L = 0.01$, 0.05, 0.10, 0.20 and 0.30 (dashed lines). The hardly visible dotted line in (*b*) represents the prediction of the linear theory for $a_w/L = 0.01$.

5.2. *Circular cavities*

The numerical method was applied to study film flow down an inclined wall with periodic depressions of various shapes. Figure 11(*a*) depicts one period of the steady surface shape for flow over a periodic sequence of semi-circular cavities with radius $R/L = 0.25$, in the absence of surfactants. Because the capillary number is high, $Ca = 20$, surface tension is insignificant. The depicted profiles correspond to film thickness $\tilde{h}/L = 0.05$, 0.10, 0.15 and 0.20, where $\tilde{h}$ is the thickness of the equivalent film over the flat portion of the wall, having a perfectly flat surface and the same area as the deformed film over each period of the wall. Figure 10(*b*) illustrates the effect of a surfactant at a lower capillary number $Ca = 2$ where surface tension is significant, for $\tilde{h}/L = 0.05$, 0.10, 0.15 and 0.20. The solid lines correspond to a clean interface or inactive surfactant, $\beta = 0$, and the dashed lines correspond to $\beta = 0.50$ and $\alpha = 100$. The surfactant is seen to accentuate the deformation of the film surface over the cavity, although the effect is small.

Figure 11(*c*) illustrates the distribution of the surfactant concentration for $\theta_0 = \pi/4$, $Ca = 2$, $\beta = 0.50$, $\alpha = 100$, corresponding to figure 11(*b*), and several equivalent film thicknesses. The corners of the cavity are located at $x/L = 0.25$ and 0.75. Marangoni tractions act to slow down the motion over the flat segments of the wall where $\mathrm{d}\Gamma/\mathrm{d}l$ is positive, and to speed up the motion above the cavity where $\mathrm{d}\Gamma/\mathrm{d}l$ is negative. A feature revealed in these graphs is that, as the film thickness increases, the amplitude in the perturbation in the surfactant concentration increases, reaches a maximum, and then decreases while obtaining a sinusoidal shape. This behaviour is consistent with the earlier results of the linear analysis for a sinusoidal wall, displayed in figure 3(*b*).

Although the surfactant has a small influence on the film deformation, it may nevertheless have a significant effect on the structure of the flow and on the streamline pattern. Figure 11(*d*) shows the distribution of the tangential velocity at the surface for $\theta_0 = \pi/4$, $Ca = 2$, $\alpha = 100$ and $\tilde{h}/L = 0.10$, reduced by the free-surface velocity U_s corresponding to $\tilde{h}$. The solid curve is for a clean interface, $\beta = 0$, and the dashed line corresponds to $\beta = 0.50$ and $\alpha = 100$; the associated surfactant concentration is plotted with the square symbols in figure 11(*c*). The deceleration of the fluid over

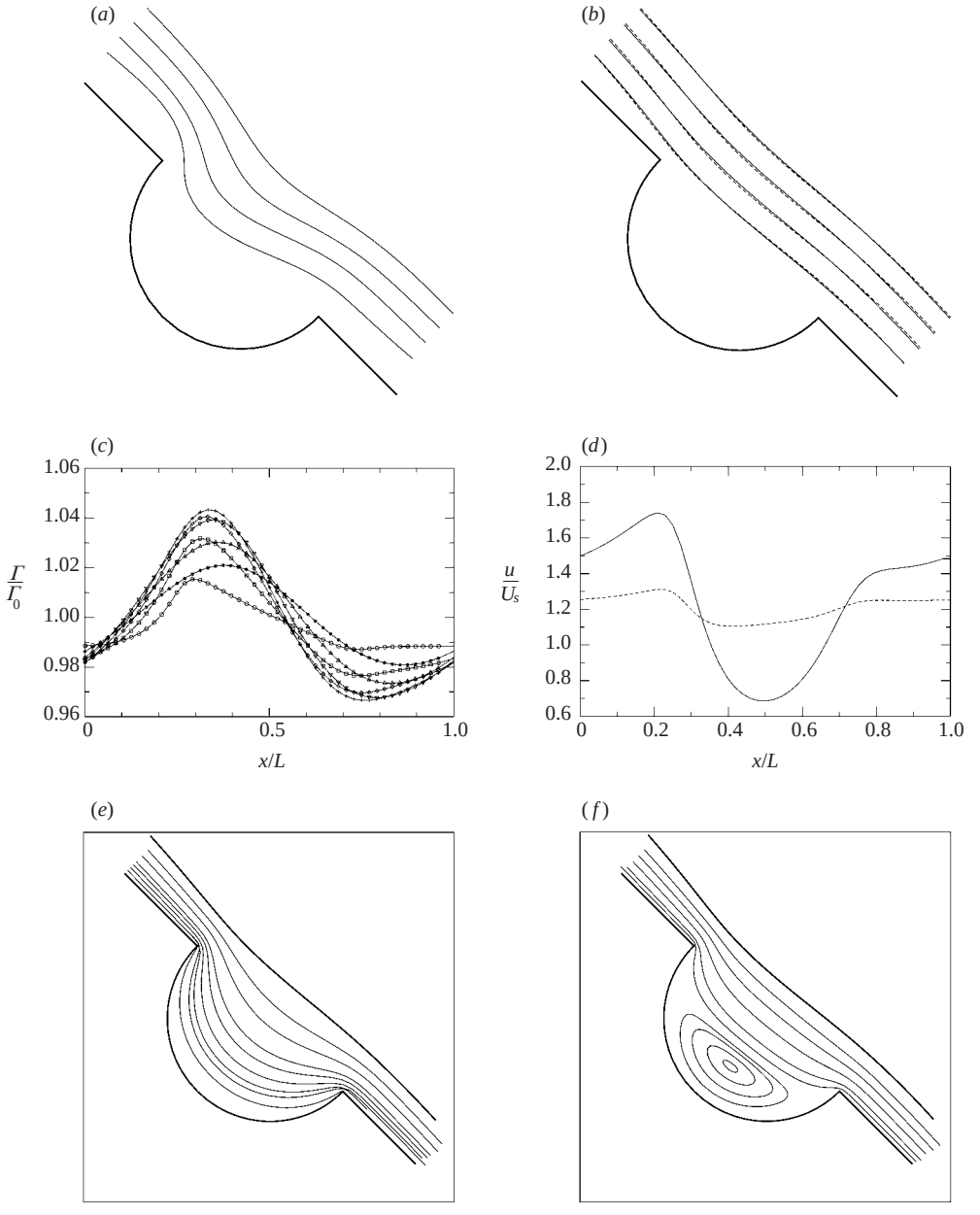

FIGURE 11. Flow over a periodic arrangement of semi-circular cavities of radius $R/L = 0.25$ for (a) $Ca = 20$ in the absence of surfactants, and (b) $Ca = 2$ and $\beta = 0$ (solid lines), or $\beta = 0.5$ $\alpha = 100$ (dashed lines). In both cases (a) and (b), the mean film thickness is $\tilde{h}/L = 0.05, 0.10, 0.15$ and 0.20. (c) Surfactant distribution for $Ca = 2$, $\beta = 0.5$ and $\alpha = 100$, and $\tilde{h}/L = 0.05$ (circles), 0.10 (squares), 0.15 (diamonds), 0.20 (crosses), 0.30 (up triangles), 0.40 (down triangles), 0.50 (stars). (d) Distribution of the tangential surface velocity for $\tilde{h}/L = 0.10$, $Ca = 2$ and $\beta = 0$ (solid line) or $\beta = 0.5$ and $\alpha = 100$ (dashed lines), and (e, f) associated streamline pattern.

the flat segments of the wall and intervening deceleration over the cavity is directly evident in this graph. As in the case of a sinusoidal wall, the surfactant renders the tangential velocity more uniform over the surface. Figure 11(e, f) shows the streamline

pattern, demonstrating the strong effect of the surfactant on the structure of the flow. In particular, the presence of the surfactant causes the onset of a nearly symmetric region of recirculating flow attached to the bottom of the cavity. The potentially important effect of flow reversal on the convective transport properties of the flow is discussed by Higdon (1985).

6. Discussion

We have found that surfactants amplify the film deformation under a broad range of conditions for small and large wall amplitudes and size of depressions, but the effect is generally moderate or small. Previous authors have studied the effect of surfactants on the deformation of a viscous drop suspended in simple shear flow, and found that the presence of surfactants is significant only when the drop viscosity is roughly less than one tenth the viscosity of the ambient liquid, the surfactant diffusivity is low and the drop aspect ratio is roughly higher then 1.5 (e.g. Yon & Pozrikidis 1998). These earlier findings are in qualitative and quantitative agreement with the present results for film flow. In contrast, we have found that the presence of the surfactant may have a profound impact on the distribution of the surface velocity and kinematics of the flow. In particular, the surfactant tends to render the tangential velocity more uniform over the film surface.

Frenkel & Halpern (2002), Halpern & Frenkel (2003) and Blyth & Pozrikidis (2003) considered the effect of a surfactant on the stability of a two-layer channel flow by linear stability analysis and numerical simulation. The results of these studies are consistent with those reported in § 4 in that, when a surfactant is present, the flow admits two normal modes, one of which is associated with the Marangoni traction. In the case of channel flow, an important parameter determining stability is the reduced shear stress of the base flow at the location of the unperturbed interface, expressed by an appropriate interface capillary number. When this reduced shear stress is zero, as in the present case of film flow, both normal modes are stable. Frenkel and Halpern found that instability of the surfactant-induced mode occurs when the interface capillary number is non-zero and the layer thickness and viscosity ratios falls within certain regions of the parameter space. When instability occurs, the Marangoni mode dominates the evolution.

Several previous authors considered the effect of surfactants on the stability of film flow. Most relevant to the present topic is the linear analysis of Lin (1970) who evaluated the critical Reynolds number for instability by carrying out a long wavenumber expansion. Unfortunately, because only one normal mode appears to survive in this limit, truncating the expansion to the second term is not sufficient for assessing the neutral growth curves and growth rates. Other authors have assumed that the surface concentration of a soluble surfactant is at equilibrium with the bulk concentration in the liquid phase, and is thus determined by bulk diffusion, evaporation and desorption (Ji & Setterwall 1994). Linear stability analysis under these conditions has revealed the occurrence of a mode of instability related to Marangoni tractions for low Reynolds numbers and moderate- or short-wavelength perturbations. These findings are consistent with the results presented in § 4 for Stokes flow. The agreement motivates the extension of the linear stability analysis for Stokes flow to Navier–Stokes flow, and this will be the topic of future work.

This research was supported by a grant provided by the National Science Foundation.

Appendix. Boundary-element method

Consider the flow of a viscous film down a periodic wall that is inclined at an angle θ_0 with respect to the horizontal, as illustrated in figure 1. We assume that the Reynolds number based on the film thickness is so small that the motion of the fluid is governed by the equations of Stokes flow.

To develop the boundary-integral formulation, we decompose the velocity and pressure into a basic component that satisfies the equations of Stokes flow with the gravity term included, denoted by the superscript B, and a disturbance component that satisfies the equations of unforced Stokes flow, denoted by the superscript D. The basic component is identified with the flat-film Nusselt solution given in (3.6), describing unidirectional flow. The no-slip and no-penetration boundary conditions require that $\boldsymbol{u}=\boldsymbol{0}$ or $\boldsymbol{u}^D=-\boldsymbol{u}^B$ over the wall. The dynamic boundary condition (2.2) requires

$$\boldsymbol{f}^D=-\boldsymbol{f}^B-(\gamma\kappa+p_a)\boldsymbol{n}-\frac{\partial\gamma}{\partial l}\boldsymbol{t} \tag{A 1}$$

over the film surface. Substituting (3.6) into (A 1), we obtain the explicit form

$$\boldsymbol{f}^D=\rho g(h-y)\begin{bmatrix}\cos\theta_0 & -\sin\theta_0\\ -\sin\theta_0 & \cos\theta_0\end{bmatrix}\cdot\boldsymbol{n}-(\gamma\kappa+p_a)\boldsymbol{n}-\frac{\partial\gamma}{\partial l}\boldsymbol{t}. \tag{A 2}$$

Further development depends on whether we consider steady or unsteady flow.

A.1. *Unsteady flow*

Applying the boundary-integral formulation for the disturbance flow, we obtain the integral equation

$$\tfrac{1}{2}u_j^D(\boldsymbol{x}_0)=-\frac{1}{4\pi\mu}\int_{W,S}G_{ij}(\boldsymbol{x},\boldsymbol{x}_0)f_i^D(\boldsymbol{x})\,\mathrm{d}l(\boldsymbol{x})+\frac{1}{4\pi}\int_{W,S}^{PV}u_i^D(\boldsymbol{x})T_{ijk}(\boldsymbol{x},\boldsymbol{x}_0)n_k(\boldsymbol{x})\,\mathrm{d}l(\boldsymbol{x}), \tag{A 3}$$

where G_{ij} is the periodic velocity Green's function of two-dimensional Stokes flow whose period is equal to that of the wall, T_{ijk} is the associated stress tensor, PV denotes the principal value of the double-layer potential, $\boldsymbol{n}$ is the unit normal vector pointing into the film, W denotes one period of the wall, S denotes one period of the film surface, and the point $\boldsymbol{x}_0$ lies on W or S. The Green's function is available in closed and readily computable form (Pozrikidis 1988, 1992). The unknowns in (A 3) are the disturbance traction over the wall and the disturbance velocity along the film surface.

Whether or not equation (A 3) has a unique solution depends on the way in which the Green's function is defined. In particular, the solution for the disturbance wall traction will be unique only if the flow rate induced by the periodic array of point forces pointing in the y-direction normal to the wall, underlying the definition of the Green's function, is non-zero. The satisfaction of this condition can be ensured by adding an arbitrary constant to the transverse component G_{yy}.

To solve the integral equation, we discretize one period of the wall into N_w elements and one period of the film surface into N_s elements, introduce approximations for the unknown functions over the elements, and apply the integral equation at element collocation points to obtain a linear system of algebraic equations (e.g. Pozrikidis 2002). In the present implementation, the disturbance velocity and traction are approximated with constant functions over the elements, and the collocation

points are placed at the element mid-points to yield the linear system

$$\boldsymbol{A}^{WW}\cdot\boldsymbol{f}^{W}+\boldsymbol{A}^{WS}\cdot\boldsymbol{f}^{S}=\boldsymbol{B}^{WW}\cdot\boldsymbol{u}^{W}+\boldsymbol{B}^{WS}\cdot\boldsymbol{u}^{S}-\tfrac{1}{2}\boldsymbol{u}^{W}, \tag{A 4}$$

for the wall collocation points, and the companion linear system

$$\boldsymbol{A}^{SW}\cdot\boldsymbol{f}^{W}+\boldsymbol{A}^{SS}\cdot\boldsymbol{f}^{S}=\boldsymbol{B}^{SW}\cdot\boldsymbol{u}^{W}+\boldsymbol{B}^{SS}\cdot\boldsymbol{u}^{S}-\tfrac{1}{2}\boldsymbol{u}^{S}, \tag{A 5}$$

for the surface collocation points. The vector $\boldsymbol{f}^{W}$ contains the x, followed by the y components of the wall disturbance traction, and the vector $\boldsymbol{u}^{W}$ contains the x, followed by the y components of the disturbance wall velocity; similarly for $\boldsymbol{f}^{S}$ and $\boldsymbol{u}^{S}$. The union of the $2N_w$ scalar equations encapsulated in (A 4) and $2N_s$ scalar equations encapsulated in (A 5) is arranged in a similar lexicographic fashion.

The influence matrices introduced in (A 4) and (A 5) are defined in terms of integrals of the single- and double-layer potential over the boundary elements. The sizes of the matrices $\boldsymbol{A}^{WW}$, $\boldsymbol{A}^{WS}$, $\boldsymbol{A}^{SW}$ and $\boldsymbol{A}^{SS}$, are, respectively, $2N_w\times 2N_w$, $2N_w\times 2N_s$, $2N_s\times 2N_w$ and $2N_s\times 2N_s$; similarly for $\boldsymbol{B}^{WW}$, $\boldsymbol{B}^{WS}$, $\boldsymbol{B}^{SW}$ and $\boldsymbol{B}^{SS}$. Moving the unknowns to the left-hand side, we obtain the $2(N_w+N_s)\times 2(N_w+N_s)$ block linear system

$$\begin{bmatrix}\boldsymbol{A}^{WW} & -\boldsymbol{B}^{WS}\\ \boldsymbol{A}^{SW} & -\boldsymbol{B}^{SS}+\dfrac{1}{2}\boldsymbol{I}\end{bmatrix}\cdot\begin{bmatrix}\boldsymbol{f}^{W}\\ \boldsymbol{u}^{S}\end{bmatrix}=\begin{bmatrix}\boldsymbol{B}^{WW}-\dfrac{1}{2}\boldsymbol{I} & -\boldsymbol{A}^{WS}\\ \boldsymbol{B}^{SW} & -\boldsymbol{A}^{SS}\end{bmatrix}\cdot\begin{bmatrix}\boldsymbol{u}^{W}\\ \boldsymbol{f}^{S}\end{bmatrix}. \tag{A 6}$$

In the present implementation, the film surface elements are straight segments, and the wall elements are either straight segments or circular arcs. The film surface normal vector and curvature are computed by cubic-spline interpolation from the position of the surface nodes, and the solution of the linear system (A 6) is found by Gauss elimination. Once the surface velocity is available, the position of the surface nodes is integrated in time using the second-order Runge–Kutta method. A simulation takes only several minutes of CPU time on an Intel 1.7 GHz processor running Linux.

To evaluate the velocity at a point $\boldsymbol{x}_0$ inside the film, we use the integral representation

$$u_j(\boldsymbol{x}_0)=u_j^{B}(\boldsymbol{x}_0)-\frac{1}{4\pi\mu}\int_{W,S}G_{ij}(\boldsymbol{x},\boldsymbol{x}_0)f_i^{D}(\boldsymbol{x})\,\mathrm{d}l(\boldsymbol{x})+\frac{1}{4\pi}\int_{W,S}u_i^{D}(\boldsymbol{x})T_{ijk}(\boldsymbol{x},\boldsymbol{x}_0)n_k(\boldsymbol{x})\,\mathrm{d}l(\boldsymbol{x}), \tag{A 7}$$

whose discrete form is

$$\boldsymbol{u}(\boldsymbol{x}_0)=\boldsymbol{u}^{B}(\boldsymbol{x}_0)-\boldsymbol{A}^{W}(\boldsymbol{x}_0)\cdot\boldsymbol{f}^{W}-\boldsymbol{A}^{S}(\boldsymbol{x}_0)\cdot\boldsymbol{f}^{S}+\boldsymbol{B}^{W}(\boldsymbol{x}_0)\cdot\boldsymbol{u}^{W}+\boldsymbol{B}^{S}(\boldsymbol{x}_0)\cdot\boldsymbol{u}^{S}, \tag{A 8}$$

where $\boldsymbol{A}^{W}$ and $\boldsymbol{B}^{W}$ are single- and double-layer influence coefficients with dimensions $2\times 2N_w$; similarly for $\boldsymbol{A}^{S}$ and $\boldsymbol{B}^{S}$. Streamlines are generated by computing the trajectories of particle paths using the modified Euler method based on the representation (A 8).

A.2. *Steady flow*

To compute the steady flow directly, we decompose the surface velocity and traction into tangential and normal components and write, for example, $\boldsymbol{B}^{SS}\cdot\boldsymbol{u}^{S}=\boldsymbol{B}_n^{SS}\cdot\boldsymbol{u}_n^{S}+\boldsymbol{B}_n^{SS}\cdot\boldsymbol{u}_t^{S}$, where the N_s-dimensional vectors $\boldsymbol{u}_n^{S}$ and $\boldsymbol{u}_t^{S}$ hold the normal and tangential components of the surface element velocities, and the $2N_s\times N_s$ matrices $\boldsymbol{B}_n^{SS}$ and $\boldsymbol{B}_n^{SS}$ arise by contracting $\boldsymbol{B}^{SS}$ using the normal and tangential vectors. Making this and

similar substitutions into (A 6), we obtain the linear system

$$\begin{bmatrix} \boldsymbol{A}^{WW} & -\boldsymbol{B}_t^{WS} & \boldsymbol{A}_n^{WS} \\ \boldsymbol{A}^{SW} & -\boldsymbol{B}_t^{SS} & \boldsymbol{A}_n^{SS} \end{bmatrix} \cdot \begin{bmatrix} \boldsymbol{f}^W \\ \boldsymbol{u}_t^S \\ \boldsymbol{f}_n^S \end{bmatrix} = \begin{bmatrix} \boldsymbol{B}^{WW} - \frac{1}{2}\boldsymbol{I} & \boldsymbol{B}_n^{WS} & -\boldsymbol{A}_t^{WS} \\ \boldsymbol{B}^{SW} & \boldsymbol{B}_n^{SS} & -\boldsymbol{A}_t^{SS} \end{bmatrix} \cdot \begin{bmatrix} \boldsymbol{u}^W \\ \boldsymbol{u}_n^S \\ \boldsymbol{f}_t^S \end{bmatrix}, \qquad (A\,9)$$

for the unknown vector on the left-hand side. The vector on the right-hand side is evaluated making use of the prescribed boundary conditions on the disturbance velocity and traction.

Because the wall and surface traction can be enhanced with an arbitrary multiple of the normal vector, system (A 9) is singular and admits an infinite number of solutions. Specifically, one of the components of $\boldsymbol{f}_n^S$ may be an inconsequential arbitrary value reflecting the unspecified level of the ambient pressure. In the present implementation, the last component of $\boldsymbol{f}_n^S$ corresponding to the last surface element, denoted by $(f_n^S)_{N_s}$, is set to zero, and the linear system is solved for the remaining $2(N_w + N_s) - 1$ unknowns. If the flow is at steady state, the solution will satisfy the boundary condition (A 1) and thus

$$\left(f_n^S + f_n^B + \gamma\kappa\right)_i - \left(f_n^S + f_N^B + \gamma\kappa\right)_{N_s} = 0, \qquad (A\,10)$$

for $i = 1, \ldots, N_s - 1$. These equations are used as objective functions to be made equal to zero with respect to variations in the y position of the $N_s - 1$ surface nodes labelled $2, \ldots, N_s - 1$, while the first surface node determining the film thickness or flow rate is held constant. The associated nonlinear algebraic system was solved by Newton's method with the Jacobian calculated by numerical differentiation.

REFERENCES

Adamson, A. W. 1990 *Physical Chemistry of Surfaces*. Wiley.

Abergel, F. & Bona, J. L. 1992 A mathematical theory for viscous free-surface flows over a perturbed plane. *Arch. Rat. Mech. Anal.* **118**, 71–93.

Blyth, M. & Pozrikidis, C. 2003 Effect of surfactants on the stability of two-layer channel flow. *J. Fluid Mech.* Submitted.

Bontozoglou, V., Kalliadasis, S. & Karabelas, A. J. 1991 Inviscid free-surface flow over a periodic wall. *J. Fluid Mech.* **226**, 189–203.

Decré, M. M. J. & Baret, J.-C. 2003 Gravity-driven flows of viscous liquids over two-dimensional topographics. *J. Fluid Mech.* **487**, 147–166.

Frenkel, A. L. & Halpern, D. 2002 Stokes-flow instability due to interfacial surfactant. *Phys. Fluids* **14**, L45–L48.

Halpern, D. & Frenkel, A. L. 2003 Destabilization of a creeping flow by interfacial surfactant: linear theory extended to all wave numbers. *J. Fluid Mech.* **485**, 67–93.

Hansen, E. B. 1986 Free surface Stokes flow over an obstacle. *Proc. Bound. Elem. VIII* (ed. Brebbia, C. A.), pp. 783–792.

Hansen, E. B. 1991 Stokes flow of a fluid layer over an obstacle on a tilted plane. *Math. Comput. Model.* **15**, 185–193.

Hayes, M., O'Brien, S. B. G. & Lammers, J. H. 2000 Green's function for steady flow over a small two-dimensional topography. *Phys. Fluids* **12**, 2845–2858.

Higdon, J. J. L. 1985 Stokes flow in arbitrary two-dimensional domains; shear flow over ridges and cavities. *J. Fluid Mech.* **159**, 195–226.

Ji, W. & Setterwall, F. 1994 On the instabilities of vertical falling liquid films in the presence of surface-active solute. *J. Fluid Mech.* **278**, 297–323.

Kalliadasis, S., Bielarz, C. & Homsy, G. M. 2000 Steady free-surface thin film flows over topography. *Phys. Fluids* **12**, 1889–1898; addendum in **12**, 3305.

Kang, F. & Chen, K. 1995 Gravity-driven two-layer flow down a slightly wavy periodic incline at low Reynolds numbers. *Intl J. Multiphase Flow* **21**, 501–513.

Lammers, J. H., O'Brien, S. B. G. & Decrè, M. M. J. 1997 Spin-coating over topography. *Proc. Second Eur. Coating Symp. Strasbourg*, pp. 278–290.

Li, X. & Pozrikidis, C. 1997 The effect of surfactants on drop deformation and on the rheology of dilute emulsions in Stokes flow. *J. Fluid Mech.* **341**, 165–194.

Lin, S. P. 1970 Stabilizing effects of surface-active agents on a film flow. *AIChE J.* **16**, 375–379.

Malamataris, N. A. & Bontozoglou, V. 1999 Computer aided analysis of viscous film flow along an inclined wavy wall. *J. Comput. Phys.* **154**, 372–392.

Mazouchi, A. & Homsy, G. M. 2001 Free surface Stokes flow over topography. *Phys. Fluids* **13**, 2751–2761.

Newhouse, L. A. & Pozrikidis, C. 1990 The Rayleigh–Taylor instability of a viscous liquid layer resting on a plane wall. *J. Fluid Mech.* **217**, 615–638.

Peurrung, L. M. & Graves, D. B. 1991 Film thickness profiles over topography in spin coating. *J. Electrochem. Soc.* **138**, 2115–2124.

Pozrikidis, C. 1988 The flow of a liquid film along a periodic wall. *J. Fluid Mech.* **188**, 275–300.

Pozrikidis, C. 1992 *Boundary Integral and Singularity Methods for Linearized Viscous Flow*. Cambridge University Press.

Pozrikidis, C. 1997 *Introduction to Theoretical and Computational Fluid Dynamics*. Oxford University Press.

Pozrikidis, C. 1998 Numerical studies of cusp formation at fluid interfaces in Stokes flow. *J. Fluid Mech.* **357**, 29–57.

Pozrikidis, C. 2001 Interfacial dynamics for Stokes flow. *J. Comput. Phys.* **169**, 250–301.

Pozrikidis, C. 2002 *A Practical Guide to Boundary Element Methods with the Software Library BEMLIB*. Chapman & Hall/CRC Press.

Pozrikidis, C. & Thoroddsen, S. T. 1991 The deformation of a liquid film flowing down an inclined plane wall over a small particle arrested on the wall. *Phys. Fluids* A **11**, 2546–2559.

Pritchard, W. G., Scott, L. R. & Tavener, S. J. 1992 Numerical and asymptotic methods for certain viscous free-surface flows. *Phil. Trans. R. Soc. Lond.* A **340**, 1–45.

Schiltz, A. 1995 An empirical model for planarization with polymer solutions. *Japan. J. Appl. Phys.* **34**, 4185–4194.

Shetty, S. & Cerro, R. L. 1993 Flow of a thin film over a periodic surface. *Intl J. Multiphase Flow* **19**, 1013–1027.

Shetty, S. & Cerro, R. L. 1998 Spreading of a liquid point source over a complex surface. *Indust. Engng Chem. Res.* **37**, 626–635.

Stillwagon, L. E. & Larson, R. G. 1990 Leveling of thin films over uneven substrates during spin coating. *Phys. Fluids* A **2**, 1937–1944.

Sukanek, P. C. 1989 A model for spin coating with topography. *J. Electrochem. Soc.* **136**, 3019–3026.

Tougou, H. 1978 Long waves on a film flow of a viscous fluid down an inclined plane wall. *J. Phys Soc. Japan* **44**, 1014–1019.

Trifonov, Y. Y. 1998 Viscous liquid film flows over a periodic surface. *Intl J. Multiphase Flow* **24**, 1131–1161.

Vlachogiannis, M. & Bontozoglou, V. 2002 Experiments on laminar film flow along a periodic wall. *J. Fluid Mech.* **457**, 133–156.

Wang, C. Y. 1981 Liquid film flowing slowly down a wavy incline. *AIChE J.* **27**, 207–212.

Wang, C. Y. 1984 Thin film flowing down a curved surface. *Z. Angew. Math. Phys.* **35**, 533–544.

Wei, H.-H. & Rumschitzki, D. S. 2002 The linear stability of a core–annular flow in an asymptotically corrugated tube. *J. Fluid Mech.* **466**, 113–147.

Yih, C.-S. 1963 Stability of liquid flow down an inclined plane. *Phys. Fluids* A **6**, 321–334.

Yon, S. & Pozrikidis, C. 1998 A finite-volume/boundary-element method for flow past interfaces in the presence of surfactants, with application to shear flow past a viscous drop. *Computers Fluids* **27**, 879–902.

Zhao, L. & Cerro, R. L. 1992 Experimental characterization of viscous film flows over complex surfaces. *Intl J. Multiphase Flow* **18**, 495–516.